Chapter 7

Defects introduced in n- and p-type Si during contacts fabrication by electron beam deposition (EBD)

7.1 Introduction

It is well known that metallization techniques, e.g. sputtering and electron beam deposition (EBD), can introduce electrically active defects at and close to the metal-semiconductor junction [1]. The electron beam deposition technique is an important device processing step as it is used to evaporate metals with melting point greater than 1500˚C. Although process induced defects on different semiconductors have been characterized before, there is still lack of understanding on the type of radiation particles that create damage during device fabrication by electron beam deposition. It is generally believed that defects introduced by EBD are due to energetic ionized residual vacuum gases generated by collision between the gas particles and the electron beam. The ionized particles are accelerated onto the sample by the electric and magnetic fields present in the EBD chamber [2]. It is important to characterize these process induced defects so as to reduce or eliminate (by annealing) those that have adverse on the device performance.

Characterization of defects introduced in Si by EBD of metals and their annealing have been previously reported [1]. A complete annealing study, which establishes the removal of all defects, is necessary in order to standardize processing conditions for obtaining a defect-free space charge region below Schottky contacts formed by EBD [3]. In this study we have used LDLTS [4,5] and DLTS [6] as the characterization techniques. LDLTS is a powerful tool which can separate defect levels with similar emission properties.

7.2 Experimental Procedure

Boron-doped Cz silicon (p-type), with carrier concentration of 1.5 x 10^{16} cm^{-3} and phosphorus – doped (n-type), with carrier concentration of 5.0 x 10^{16} cm^{-3} were used for this study. The samples were cut into 1 cm x 0.4 cm sizes before cleaning. Prior to metallization the samples were chemically cleaned by degreasing in boiling trichloroethylene and then in boiling iso-propanol followed by an etching step in dilute HF, i.e. HF:H_2O (1:6) to remove the oxide layer. The samples were then rinsed in de-ionized water and blow-dried in nitrogen and thereafter immediately loaded into the vacuum chamber which was evacuated to a pressure of below 1 x 10^{-6} mbar to reduce oxide build-up before metallization.

On the p-type samples, titanium and then molybdenum, 100 nm thick each, were deposited through a circular mask of 0.48 mm in diameter, using electron beam deposition. The source of electron beam is a VARIAN 10 kW e-gun which employs a 10 kV (1 A) power source for the anode and a filament current of 40 A at 10 V. An electric field and magnetic field focus and accelerate the electric beam to the target metal. In-Ga eutectic was rubbed on the back-surface of the sample as the ohmic contact.

Similarly, on n-type samples, cobalt (Co), platinum (Pt), or ruthenium (Ru) Schottky contacts were fabricated through a circular of 0.48 mm in diameter using electron beam deposition. In-Ga eutectic was used as the back-surface ohmic contact.

After metallization current-voltage (*I-V*) and capacitance-voltage (*C-V*) were used to extract the free carrier concentration and monitoring the quality of the diodes. To determine the signature of the defects induced by electron beam deposition, DLTS and Laplace (LDLTS) were used. The defect 'signatures' (i.e. activation enthalpy in eV for holes or electrons E_T, and apparent capture cross-section, σ_a) were determined from Arrhenius plots of $\ln(T^2/e)$ vs. $1000/T$, where e is either the hole or electron emission rate and T is the measurement temperature. To shed more light on the structure and identity of defects, isochronal annealing cycles were done from room temperature up to 600˚C. The defect depth profiles (i.e. defect concentration versus

depth) were obtained by fixed bias - variable pulse method with the edge region correction suggested by Zohta and Watanabe [7].

7.3 Results

The electrical characteristics of the defects introduced during metallization by electron beam deposition on n-type and p-type silicon is presented in this section. DLTS and LDLTS have been used to probe the defect electronic properties and depth profiles below the semiconductors surface.

7.3.1 Electron beam deposition induced defects in p-type silicon

Defects introduced during metallization, revealed by a DLTS spectrum in Fig. 7-1, curve (a) are *H*(0.17), *H*(0.23), *H*(0.37) and *H*(0.49). In this nomenclature "*H*" means "hole trap" and the number after *H* is the activation energy, in eV, obtained from the Arrhenius plots shown in Fig. 7-3. The electronic properties of the defects introduced during EBD are summarized in Table. 7.1.

Table 7.1. Electronic properties of defects introduced during EBD of Ti/Mo contacts on B-doped Cz Si

Defect	E_T (eV)	σ_a (cm^2)	T_{peak} [a] (K)	T_{in} [b] (°C)	T_{out} [c] (°C)	Defect identity
After	*electron*	*beam*	*deposition*			
H(0.17)	0.17	6.1 x 10^{-16}	100	RT	450	?
H(0.23)	0.23	1.7 x 10^{-15}	150	RT	400	H-related [8]
H(0.37)	0.37	1.5 x 10^{-15}	192	RT	450	C_I-O_I [8,9,10]
After	*annealing*					
H(0.39)	0.39	4.3 x 10^{-16}	213	350	450	?
H(0.49)	0.49	1.0 x 10^{-15}	265	350	550	B-H?

[a] Peak position at a rate window of 80 s^{-1}. [b]Temperature at which the defect is introduced. [c]Temperature at which the defect is removed.

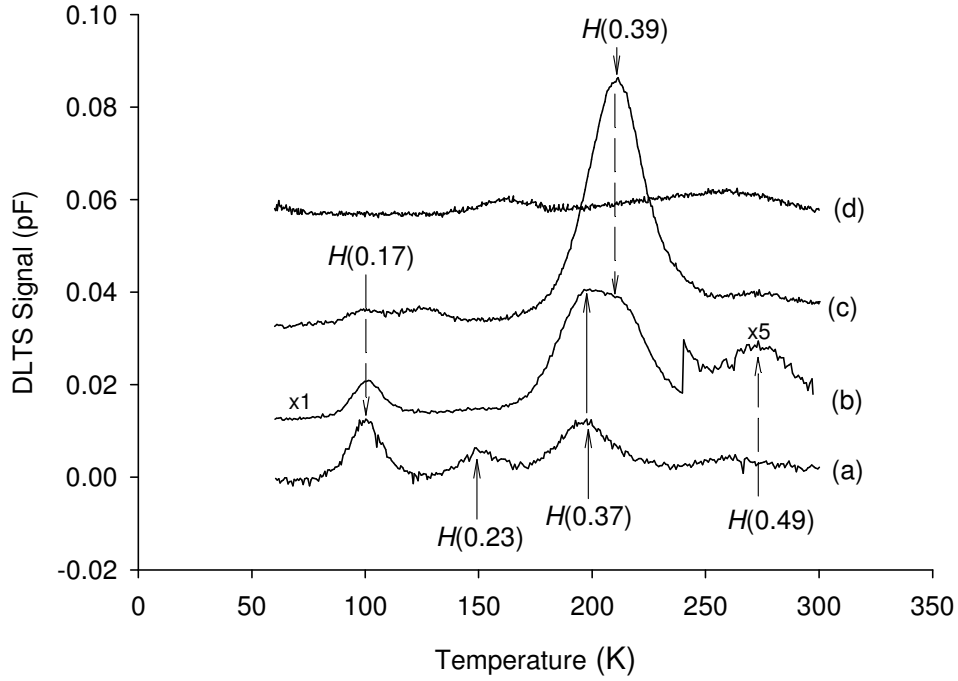

Fig. 7-1. DLTS spectra of the defects present in the depletion layer below the Ti/Mo Schottky contact on p-type Si (a) after deposition and after annealing at (b) 400˚C, (c) 450˚C, and (d) 550˚C. The spectra were recorded at an emission rate of 80 s^{-1}, a quiescent reverse bias of -2 V and a filling pulse amplitude of 2.2 V.

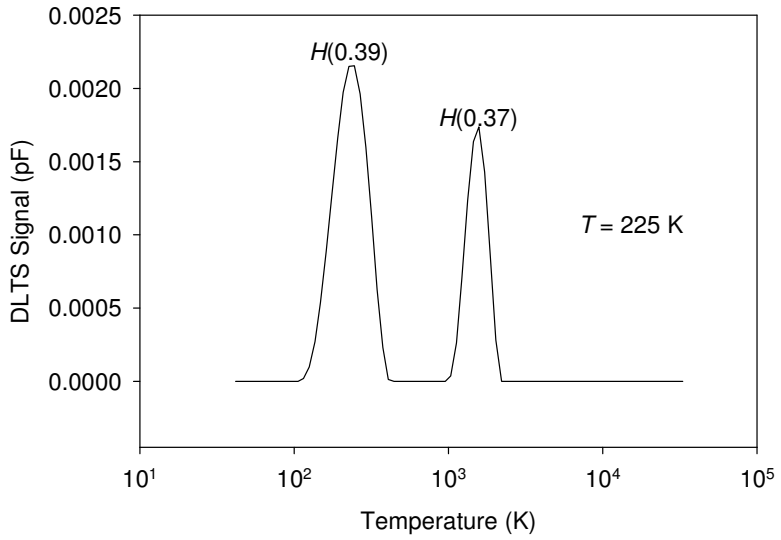

Fig. 7-2. LDLTS spectrum of the peak marked "H(0.37) + H(0.39)", recorded at 225 K. LDLTS clearly separates the signals of the two defects.

It should be pointed out that these defects were not observed in identical silicon samples on which Ni Schottky contacts were fabricated by resistive evaporation. All

the defects are therefore introduced by EBD. The annealing behavior of defects introduced by electron beam deposition of Ti/Mo is presented in Fig. 7-2, curves (a-d). Annealing at 400˚C removed *H*(0.23) (curve(b)), while *H*(0.17) and *H*(0.37) were removed after annealing at 450˚C (curve(c)). The defect level *H*(0.39) was introduced at 350˚C and its concentration reached a maximum at 450˚C and thereafter it annealed out at 550˚C. After annealing at 400˚C, LDLTS was used to separate the traps *H*(0.37) and *H*(0.39) which was not possible with DLTS as shown in Fig. 7-2. After annealing at 550˚C and higher temperatures, no defect peaks could be detected within the detection limit of our system.

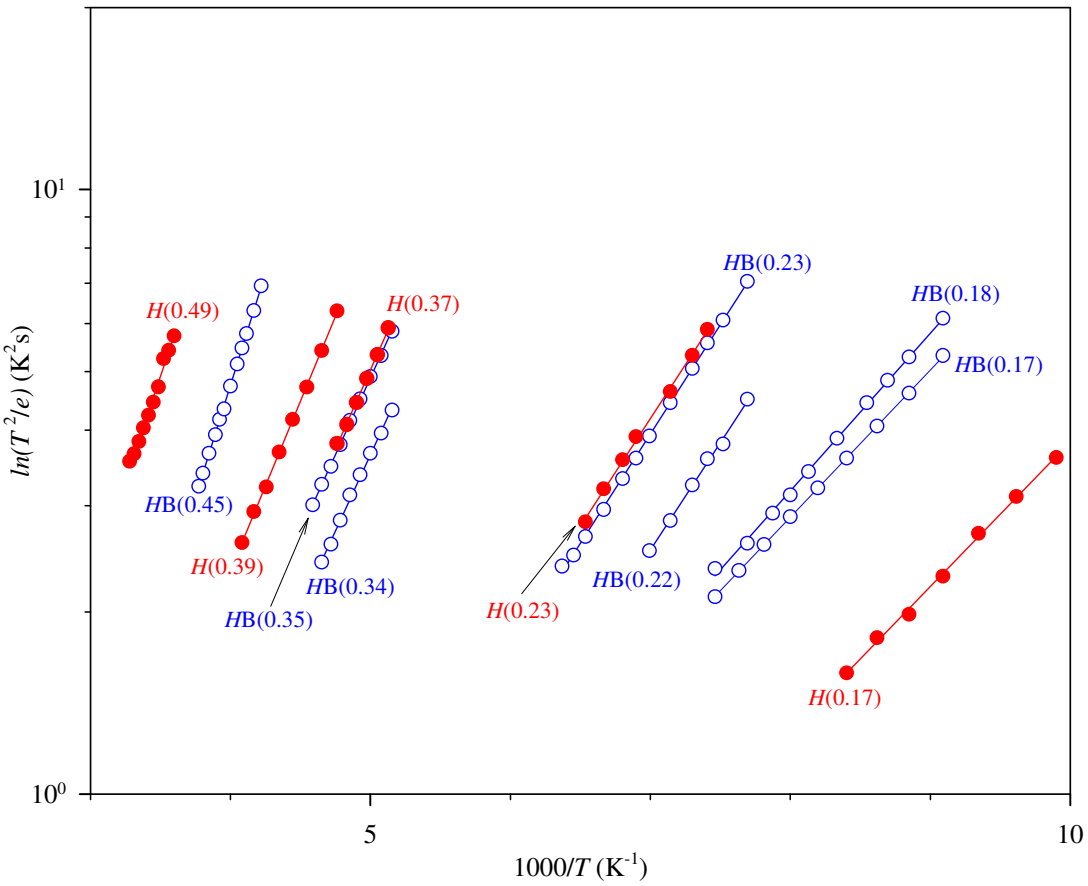

Fig. 7-3. Arrhenius plots of the defects present in the depletion layer below the Ti/Mo Schottky contact on B-doped Si after deposition (red circles) compared to the defects introduced in similar samples after 1 MeV electron irradiation (blue circles).

As shown in Table 7.1 and Arrhenius plots in Fig. 7-3, most of these defects have different properties to those introduced by electron irradiation of similar samples

presented in chapter 6. *H*(0.23) has been attributed to a H- related defect [8] which is similar to a defect level *H*B(0.23) discussed in chapter 6. *H*(0.37) has similar electronic properties to the C_I-O_I. A defect at E_V + 0.35 eV with a similar annealing behavior has also been reported by Auret *et al* after electron irradiation of p-type Si, as well as after EBD of contacts on p-type Si [9]. It has been convincingly demonstrated that this level is associated with the C_I-O_I [10]. *H*(0.39) may be a defect that forms as the C_I-O_I breaks up during annealing [10]. The nature of *H*(0.49) is not clear at the moment. It should be pointed out, however, that Mooney *et al* [8] and Auret *et al* [9] observed levels at E_V + 0.48 eV and E_V + 0.49 eV, respectively, in electron irradiated, B-doped Si. Although the trap level *H*(0.17) has similar energy level to the divacancy it should be pointed out that the level observed here has different structure and properties to the divacany as evidenced by the Arrhenius plots in Fig. 7-3 and also it anneals out at a much higher temperature than the annealing range (250˚C - 300˚C) of the divacancy [11].

DLTS depth profiles of EBD induced defects indicated that the concentration of all the defects decreased from the surface into the Si away from the junction (examples of such profiles have been presented in section 7.3.2). This is due to the fact that EBD introduces defects at and below the surface, which will then diffuse deeper into the material and form more stable complexes [1]. These defects have been shown to be caused by energetic particles accelerated from the vicinity of the electronic filament onto the sample by the electric and magnetic fields present in the vicinity of the metal source [2].

To shed more light on the source of defects during the deposition process, TRIM (version 2006.02) [12] simulations are presented here. Figs. 7-4 (a-d) show the TRIM simulation of the ion ranges and damage created by several common residual vacuum gases, which are thought to be responsible for the damage on substrate surface during electron beam deposition. For a maximum ion energy of 10 keV (which is expected in our electron beam deposition system), the projected ion range for C, O, and N is on average ~30 *n*m producing on approximately, 3 vacancies/ion/*n*m, whereas H ions of the same energy will have a projected range of 132 *n*m and each ion producing 18 x 10^{-3} vacancies/*n*m. Therefore it is expected that the primary damage will be very close to the semiconductor surface and the vacancy-interstitial pairs created will then

diffuse until they form stable complex defects. Considering the number of vacancies/*n*m created during EBD the formation of higher order vacancies or interstitial complexes is possible.

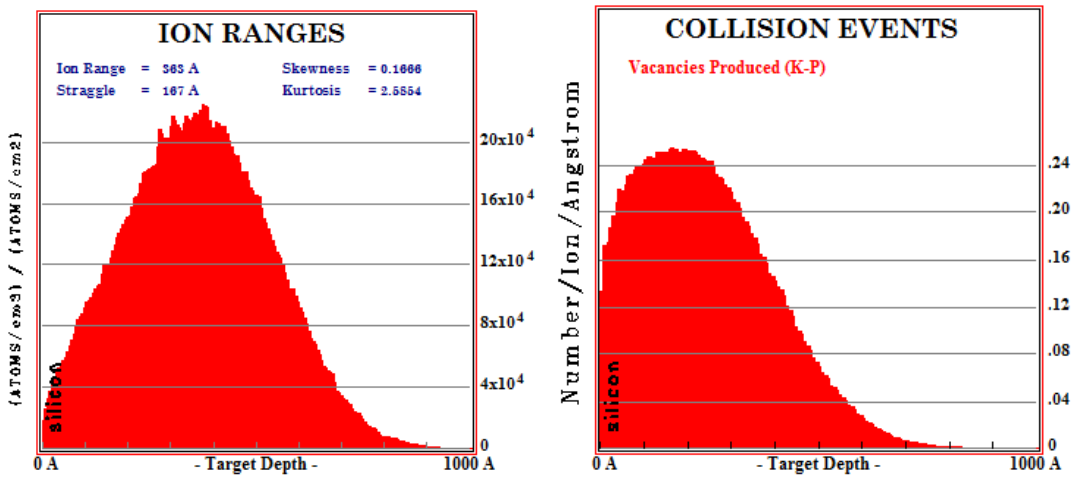

(i) (ii)

Fig. 7-4 (a). (i) TRIM simulation for the projected range and (ii) damage events of 10 keV carbon ions in silicon.

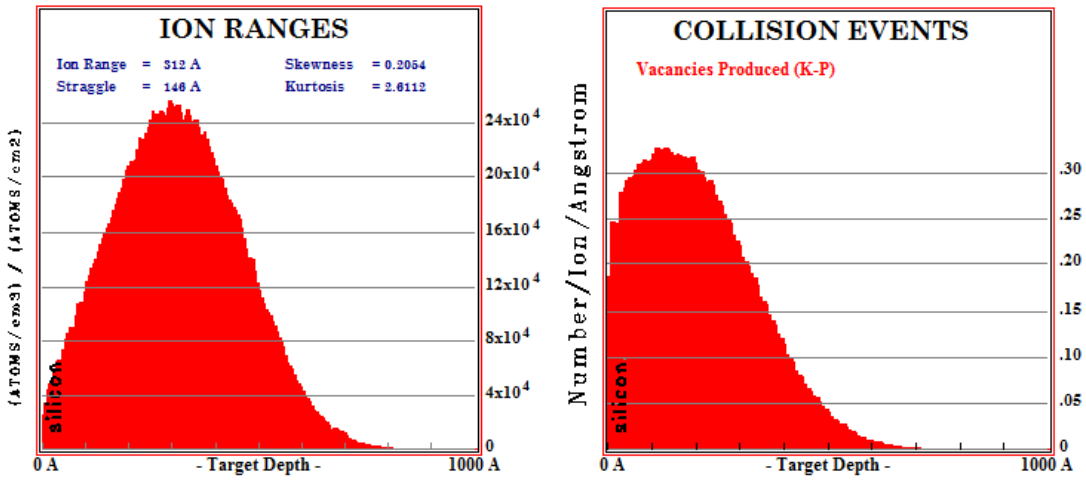

(i) (ii)

Fig. 7-4 (b). (i) TRIM simulation for the projected range and (ii) damage events of 10 keV nitrogen ions in silicon.

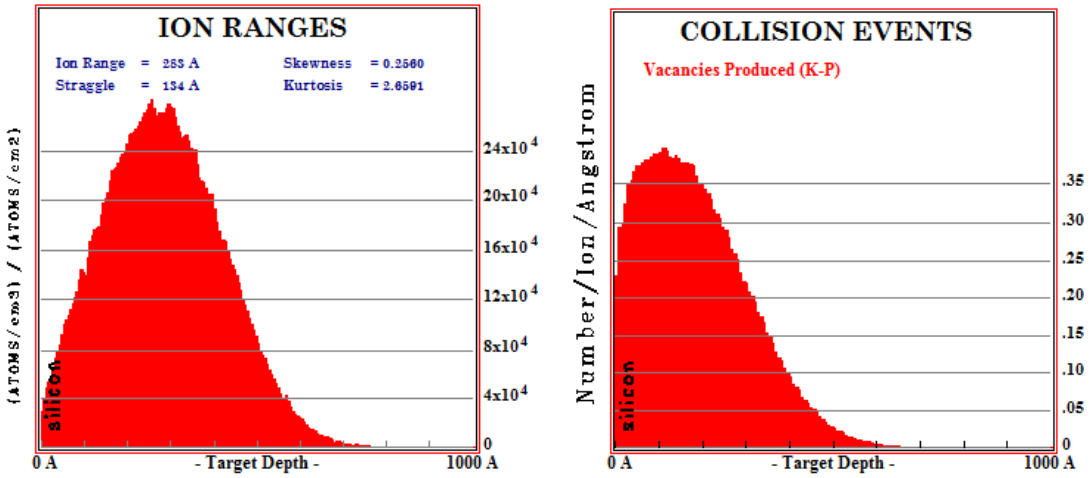

(i) (ii)

Fig. 7-4 (c). (i) TRIM simulation for the projected range and (ii) damage events of 10 keV oxygen ions in silicon.

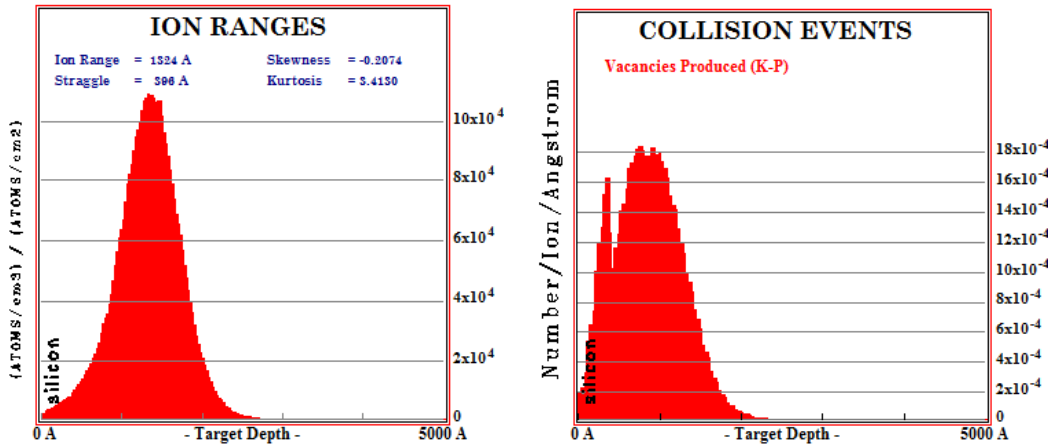

(i) (ii)

Fig. 7-4 (d). (i) TRIM simulation for the projected range and (ii) damage events of 10 keV hydrogen ions in silicon.

7.3.2 Electron beam deposition induced defects in n-type silicon

After the electron beam deposition of Ru Schottky barrier diodes, the defect levels *E*(0.45), *E*(0.42), *E*(0.22), *E*(0.15) and *E*(0.05) were introduced as shown in Fig. 7-5 (a). In this nomenclature, "*E*" is electron trap and the number '0.45' is the activation enthalpy (in eV). There were no defect levels observed within the detectable limit of our DLTS system in the same samples after metallization of Ni Schottky contacts by resistive evaporation. Defect *'signatures'* for the EBD induced defects which were extracted from the Arrhenius plots shown in Fig. 7-8 are

summarized in Table 7-2. The EBD induced defects have been compared to those introduced by MeV irradiation of similar samples.

Table 7.2. Electronic properties of defects introduced during EBD of Ru contacts on P-doped Si and those introduced by MeV electron irradiation in similar samples.

Defect	E_T (eV)	σ_a (cm^2)	T_{peak} [a] (K)	Defect	E_T (eV)	σ_a (cm^2)	T_{peak} [a] (K)	Defect identity
Electron	*beam*	*deposition*		*MeV*	*electron*	*irradiation*		
E(0.45)	E_C - 0.45	1.3 x 10^{-14}	215	E(0.46)	E_C -0.46	1.5 x 10^{-14}	215	V-P [2,13,14]
E(0.42)	E_C - 0.42	4.1 x 10^{-14}	205	E(0.43)	E_C -0.43	3.0 x 10^{-14}	205	$V_2^{-/0}$ [2,13,14]
E(0.22)	E_C - 0.22	9.0 x 10^{-15}	123	E(0.24)	E_C -0.24	7.8 x 10^{-15}	123	$V_2^{=/-}$ [13,14]
				E(0.17)	E_C -0.17	1.1 x 10^{-14}	90	V-O [13,14,15]
				E(0.14)	E_C -0.14	1.6 x 10^{-13}	67	C_s-Si_i ?
E(0.15)	E_C - 0.15	2.5 x 10^{-15}	83					?
E(0.05)	E_C - 0.05	1.4 x 10^{-19}	57					?
After	*annealing*							
E(0.28)	E_C - 0.28	8.6 x 10^{-17}	180					C_i -? [13,15,16]
E(0.18)	E_C - 0.18	3.8 x 10^{-16}	110					?

[a] Peak position at a rate window of 80 s^{-1}.

E(0.45) is the well known vacancy-phosphorus (E-center) and E(0.42) has similar electronic characteristics to the single charge state of the divacancy, while E(0.22) is attributed to the double charge state of the divacancy [2,13,14]. These two traps have similar structures to E(0.46) and E(0.43) observed after MeV electron irradiation. The E(0.42) and E(0.45) were successfully separated using LDLTS as shown in Fig. 7-6.

The origin of *E*(0.15) and *E*(0.05) is still subject to speculation at the moment. After annealing the defects were monitored by DLTS as shown in Figs. 7-5 and 7-7.

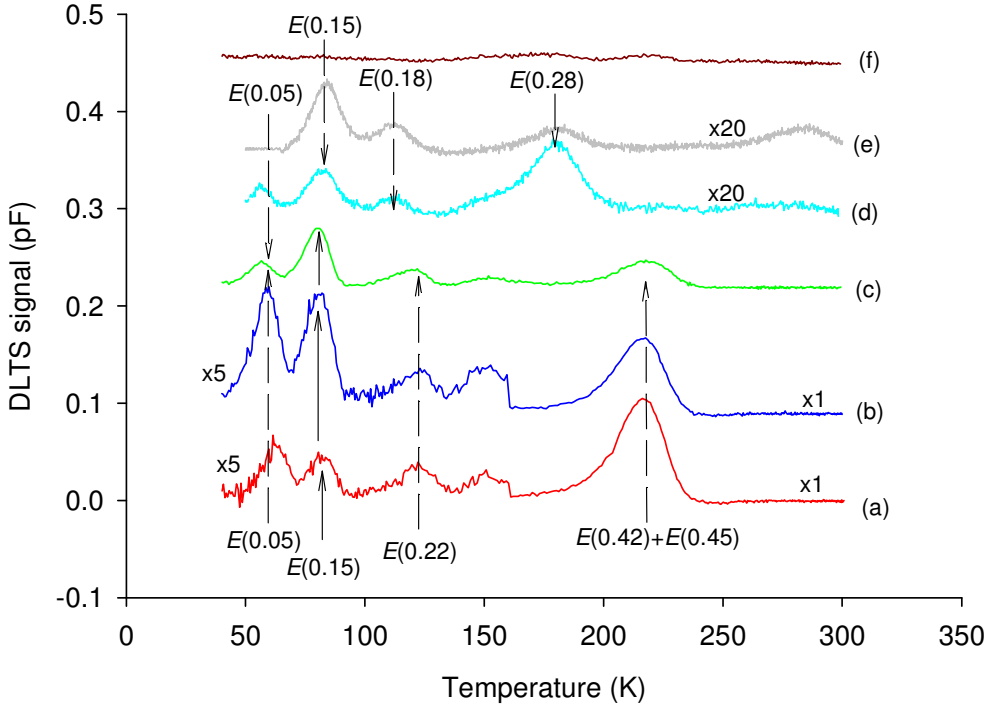

Fig. 7-5. DLTS spectra of defects introduced in P-doped Si after Ru Schottky contacts fabrication using EBD for (a) for as-deposited sample, and after annealing at (b) 150°C, (c) 250°C, (d) 350°C, (e) 400°C and (f) 450°C. The spectra were recorded at a quiescent reverse bias of -2 V, a filling pulse of 1.2 V and rate window (RW) of 80 s^{-1}.

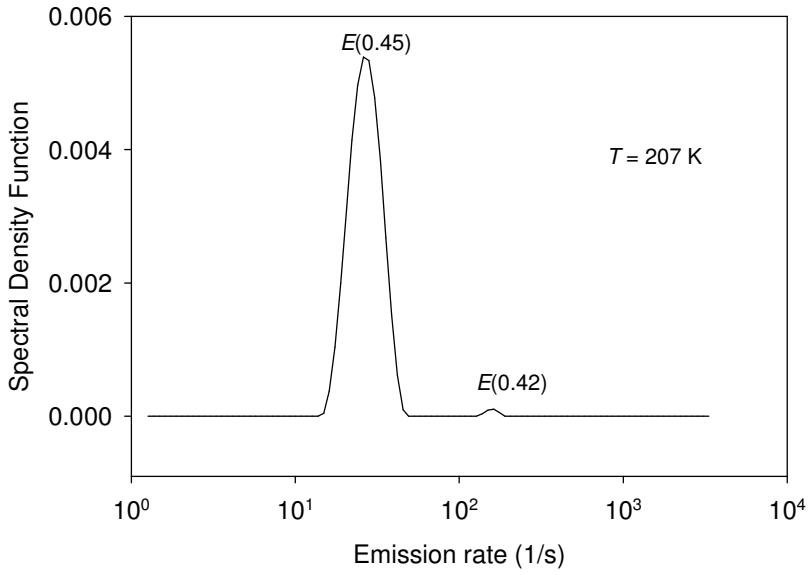

Fig. 7-6. LDLTS spectra for the levels E(0.45) and E(0.37) recorded at 207 K.

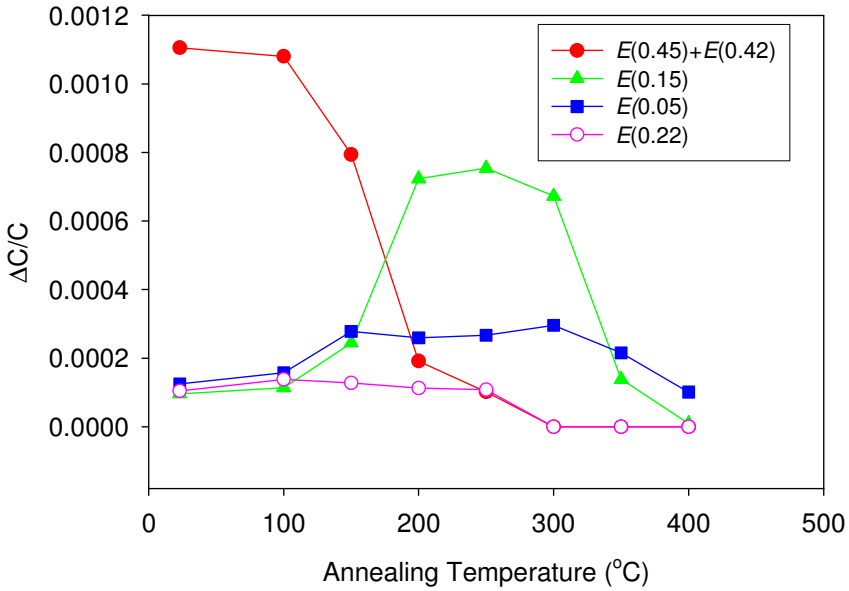

Fig. 7-7. Annealing behaviour of primary defects introduced in p-type silicon by electron beam deposition.

Annealing at above 250˚C, *E*(0.18) and *E*(0.28) were introduced, and *E*(0.18) has a different structure to the trap level *E*(0.17) assigned to the V-O (A-center) which was observed after electron irradiation as evidenced by the Arrhenius plots in Fig, 7-8, while *E*(0.28) is thought to be interstitial carbon- related [15,16]. Electron irradiation introduced the level *E*(0.14) which has different structure to *E*(0.15) observed after electron beam deposition. The depletion layer was defect-free after annealing at 550˚C or higher.

Depth profiling of the *E*-center shows a decrease in defect concentration with depth from the semiconductor surface as shown in Fig. 7-9, which is characteristic of damage caused by heavy energetic particles whose energy decreases with depth. The depth profiles of defects introduced after Ru and Pt Schottky contacts fabrication on the similar samples using EBD are depicted in Fig. 7-9 curves (a) and (b) respectively. The defect concentration at the semiconductor surface is higher for Ru than for Pt. This is attributed to the fact that Ru has a higher melting point (2250˚C) than Pt (2041˚C), hence during Ru deposition a higher filament current is used, therefore the particles in the vicinity of the filament will have a higher flux (than in case of Pt deposition) creating much more damage on and beneath the semiconductor surface.

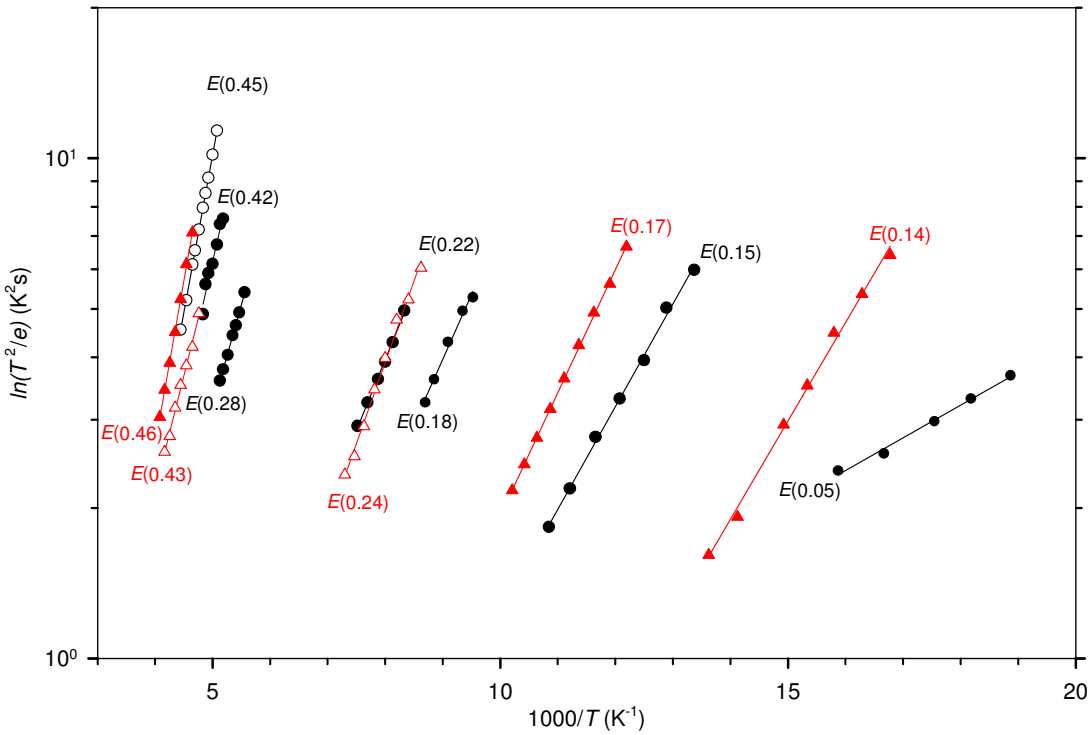

Fig. 7-8. Arrhenius plot of defects in P-doped Si after Ru Schottky contacts fabrication using EBD (black circles) and after 1 MeV electron irradiation (red triangles).

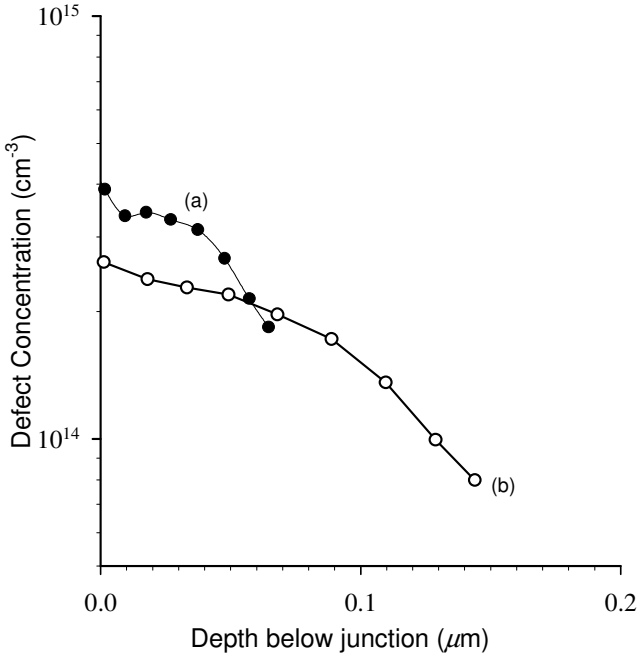

Fig. 7-9. Depth profile of E-center after (a) Ru (b) Pt Schotky contacts fabrication P-doped Si using EBD. Measurements were recorded using a fixed bias of -2 V and a variable pulse method, ref. 7.

7.4 Summary and Conclusions

Defects introduced during metallization on B-doped, and P-doped Si using EBD have been characterized by DLTS and LDLTS, and compared to those introduced by MeV electron irradiation in similar samples. The thermal stability of EBD induced defects have been investigated in the temperature range (100˚C – 600˚C). In case of p-type Si the Mo that was added on top of the Ti prevented annealing degradation of the Ti contact with the semiconductor at higher annealing temperatures. DLTS revealed that the main defects introduced during metallization are hole traps *H*(0.17), *H*(0.23), and *H*(0.37). After annealing two secondary defects *H*(0.39) and *H*(0.49) were observed. The trap *H*(0.37) has been assigned to the C_I-O_I and *H*(0.23) is hydrogen-related. The structure of *H*(0.17) seems to have a different structure to that of the single charged donor state of the divacancy while the origin of both *H*(0.39) and *H*(0.49) is still not clear. After annealing at 550˚C and higher a defect-free depletion region was obtained. LDLTS was successfully used to deconvolute signals of *H*(0.37) and *H*(0.39) defects which are both present after annealing at above 400˚C. It was concluded that electron beam deposition introduces some defects which are common to those introduced by high energy electron irradiation.

In phosphorus-doped Si, the primary defects introduced by EBD were *E*(0.45), *E*(0.42), *E*(0.22), *E*(0.15), and *E*(0.05). The closely spaced traps *E*(0.45) and *E*(0.42) were separated by LDLTS. *E*(0.45) has been identified as the V-P (*E*-center) while *E*(0.42) and *E*(0.22) have been identified as the single and double acceptor charge states of the divacancy, respectively. Upon annealing the defect levels *E*(0.18), and *E*(0.28) were observed. *E*(0.18) has a different structure to the trap *E*(0.17) observed after electron irradiation and assigned to the V-O (A-center). *E*(0.28) has been identified as being C_i- related. The identity of *E*(0.05) and *E* (0.15) is not clear at the moment. A defect-free depletion region was observed after annealing at 550˚C and higher. The depth profile of the, *E*-center (*E*(0.48)), showed a high concentration of the defects close to the metal - semiconductor surface and concentration decreasing with depth into the material.

References

[1] F.D. Auret and P.M. Mooney, *J. Appl. Phys*. Vol. **55** (1984) 984.

[2] C. Christensen, J.W. Petersen and A.N. Larsen, *Appl. Phys. Lett*. Vol. **61** (1992) 1426.

[3] F.D. Auret, A.G.M. Das, C. Nyamhere, M. Hayes and N.G. van der Berg, *Solid State Phenomena* **108-109** (2005) 561.

[4] L. Dobaczewski, P. Kaczor, I.D. Hawkins and A.R. Peaker, *J. Appl. Phys*. **76** (1994) 194.

[5] L. Dobaczewski, A.R. Peaker and K.B. Nielsen, *J. Appl. Phys*. **96** (1994) 4689.

[6] D.V. Lang, *J. Appl. Phys*. **45** (1974) 3023.

[7] Y. Zohta and M.O. Watanabe, *J. Appl. Phys*. **53** (1982) 1809.

[8] Y. Tokuda and H. Sato, *Mater. Scie. In Semiconductor Processing*, **6** (2003) 277.

[9] F.D. Auret and P.M. Mooney, *J. Appl. Phys*. **55** (1984) 984.

[10] J.M. Trombetta and G.D. Watkins, *Appl. Phys. Let*t. **51** (1987) 1103.

[11] K. Nishimura, M. Yamaguchi, O. Anzawa, T.K. Vu, A. Khan, Y. Ohshita, T. Abe, M. Imaizumi, S. Matsuda, T. Ohshima and H. Itoh. *3rd World Conference on Photovoltaic Energy Conversion*, May 11-18, 2003 Osaka, Japan plenary, Oral.

[12] J.P. Biersack and L.G. Haggmark, *Nucl. Instrum. Methods* **174** (1980) 257.

[13] P. Pellegrino, A. Y. Kuznestov and B.G. Svensson, *Physica B*, **273-274** (1999) 489.

[14] J. Lalita, N. Keskitalo, A. Hellén, C. Jadadisn and B.G. Svensson, *Nuclear Intruments and Methods in Physics Research* B ***120*** (1996) 27.

[15] P. Lévêque, A. Hallen, P. Pellegrino, B.G. Svensson and V. Privitera, *Nucl. Instr. and Meth. Phys. Res. B* **186** (2002) 375.

[16] J. Stahl, E. Fretwirst, G. Lindstrom and I. Pintilie, *Nucl. Instr. and Meth. A* **512** (2003) 111.

List of Publications

1. F.D. Auret, A.G.M. Das, C. Nyamhere, M. Hayes and N.G. van der Berg; "*Thermal Stability of Ti/Mo Schottky contacts on p-Si and Defects Introduced in p-Si During Electron Beam Deposition of Ti/Mo*", Solid state Phenomena, vols. **108-109** (2005) 561-566.
2. Cloud Nyamhere, A. Chawanda, A.G.M. Das, F.D. Auret and M. Hayes, "*Thermal stability of Co, Ni, Pt or Ru Schottky contacts on n-Si and defects introduced thereon during contacts fabrication using electron beam deposition*", Physica B, Vols. **401- 402** (2007) 226 - 229.
3. C. Nyamhere, A.G.M. Das, F.D. Auret and M. Hayes, "*Deep Level Transient Spectroscopy Characterisation of Defects Introduced in p-Si Electron Beam Deposition and Proton Irradiation*", Journal of Physics, Conference Series, vol.**100** (2008), 042004.
4. A.G.M. Das, C. Nyamhere and F.D. Auret "A Comparitive Study of electronic properties of defects introduced in p-Si (i) During Electron Beam Deposition of *Ti/Mo, (ii) by proton irradiation and (iii) by electron irradiation*", Surface and Coatings Technology, Vol. **203** (2009) 2628-2631.

Chapter 8

Radiation-induced defects in antimony-doped germanium after electron irradiation

8.1 Introduction

There is growing interest in Germanium (Ge) as a possible candidate for high performance complimentary metal-oxide-semiconductor (CMOS) devices because of its higher mobility when compared to silicon (Si) at low electric fields [1-2]. This has led to renewed interest in the complete understanding of origins and dynamic properties of radiation and process induced defects in Ge. Although several authors [3,4,5,6,7,8] have studied radiation defects introduced intentionally, by radiation or unintentionally, during processing stages, there is lack of understanding of the origins of most defects. In this chapter we have characterized defects, deliberately introduced by electron irradiation in n-type Ge doped with Sb using DLTS and LDLTS. The annealing characteristics of the defects are also presented to shed more light on the defect origin. Also presented in this chapter are the depth profile and the introduction rates of the *E*-center.

8.2 Experimental Procedure

Three sets of samples, (labeled Ge110, Ge111 and Ge100), of n-type, bulk grown Ge doped with Sb and supplied by Umicore have been used in this investigation. In the sample label nomenclature 'Ge110', Ge is germanium, 110 is the sample orientation. The doping levels were 2.2 x 10^{14} cm^{-3}, 1.0 x 10^{15} and 2.6 x 10^{15} for Ge110, Ge111 and Ge100 respectively. Before metallization the samples of 1cm x 1cm in size were first degreased and then etched in a mixture of H_2O_2:H_2O (1:5) for 1 minute. Immediately after cleaning they were inserted into a vacuum chamber where AuSb (0.6% Sb) was deposited by resistive evaporation process, on their back surfaces as ohmic contacts. The samples were then annealed at 350˚C in argon (Ar) for 10

minutes to reduce the contact resistivity of the ohmic contacts. Before the Schottky contact fabrication, the cleaning procedure above was repeated. Au contacts, 0.60 mm in diameter and 200 nm thick were deposited by vacuum resistive evaporation process. After the contact formation the samples were characterized by current – voltage (*I-V*) and capacitance – voltage (*C-V*) measurements at room temperature to determine the quality of the diodes. The samples were then irradiated by MeV electrons from a ^{90}Sr radionuclide source at different fluences. The energy distribution from this source is continuous with a primary peak energy of about 200 keV, a secondary maximum of about 1 MeV, and then it tails off to about 2 MeV [3]. After each and every dose the defects introduced were measured by DLTS and Laplace – DLTS. The current - temperature (*I-T*) and capacitance - temperature (*C-T*) measurements were also recorded. The '*signatures*' of radiation induced defects (i.e. activation enthalpy for the electron traps and hole traps, E_T, and apparent capture cross section, σ_a), were determined from Arrhenius plots of $ln(T^2/e)$ vs. $1000/T$, where 'e' is either the hole or electron emission rate, and T is the measurement temperature.

In order to investigate the defect annealing behaviour, the irradiated samples were annealed isochronally for 20 minutes in Ar gas from room temperature up to 500˚C.

8.3 Results

In this section the electronic and annealing properties of hole traps created in the samples after electron irradiation are discussed. The evolution of defects with increase in fluence and defects created in samples of different doping concentrations are revealed.

8.3.1 Defects introduced in Ge after electron irradiation with different doses

DLTS spectra of defects introduced in n-Ge after MeV electron irradiation at various doses are depicted in Fig. 8-1 and the defect 'signatures' extracted from Arrhenius plots (shown Fig. 8-4) are summarised in Table 8.1. No defect levels were detected within detection limit (about 10^{11} cm^{-3}) of our experimental system for the as-deposited samples, as shown in Fig. 8-1 (curves (a_e) and (a_h)). In the nomenclature

used here to label the curves, the subscripts 'e' and 'h' indicate that the spectrum is for electron traps and hole traps respectively.

Table 8.1. A summary of defects electron properties introduced in n-type Ge by electron irradiation.

Defect	E_T (eV)	σ_a (cm^2)	T^a_{peak} (K)	T^b_{out} (°C)	Defect origin
E(0.15)	$E_C - 0.15$	3.1 x 10^{-13}	78	150	Sb related?
E(0.20)	$E_C - 0.20$	2.3 x 10^{-13}	100	150	Sb and I related [2-4]
E(0.21)	$E_C - 0.21$	1.1 x 10^{-13}	101	150	Sb related [2-4]
E(0.23)	$E_C - 0.23$	9.7 x 10^{-13}	132	175	Sb and I related [2-4]
E(0.31)	$E_C - 0.31$	3.1 x 10^{-13}	151	125	I and impurity related [2-4]
E(0.38)	$E_C - 0.38$	6.1 x 10^{-14}	191	200	V-Sb (--/-) [2-6]
H(0.30)	$E_V + 0.30$	4.0 x 10^{-12}	142	200	V-Sb (0/-) [2-4]

[a]Peak temperature at a rate window of 80 s^{-1}, [b]Temperature at which defect is removed.

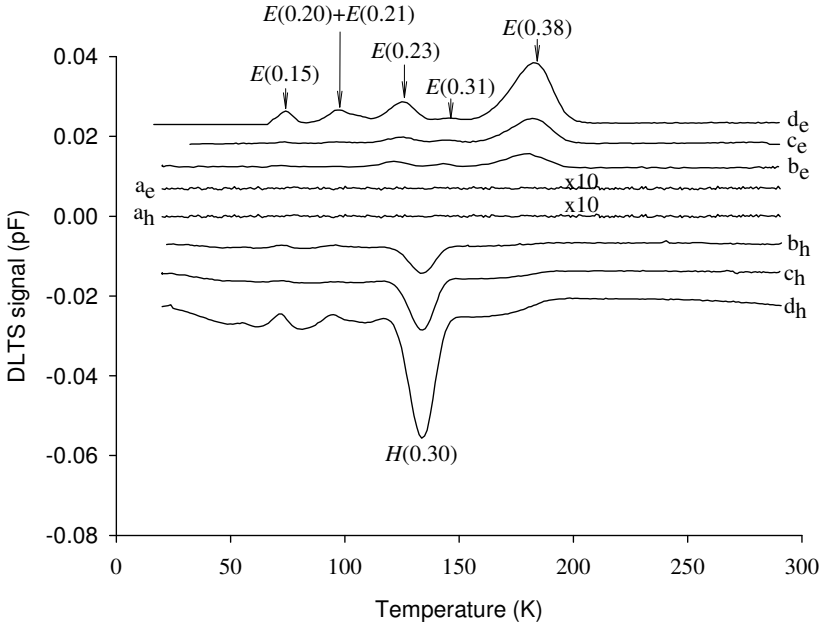

Fig. 8-1. DLTS spectra for sample Ge100 (a) as-deposited and after MeV electron irradiation at fluences of (b) 1.4 x 10^{13} e cm^{-2}, (c) 3.7 x 10^{13} e cm^{-2}, and (d) 9.2 x 10^{13} e cm^{-2}. The subscripts 'e' and 'h' on the graph labels stand for electron and hole traps respectively. These spectra were recorded at a rate window of 80 s^{-1} and quiescent reverse bias of -2 V with a filling pulse of 0 V and 3 V for electron and hole traps, respectively and a pulse width of 1 ms.

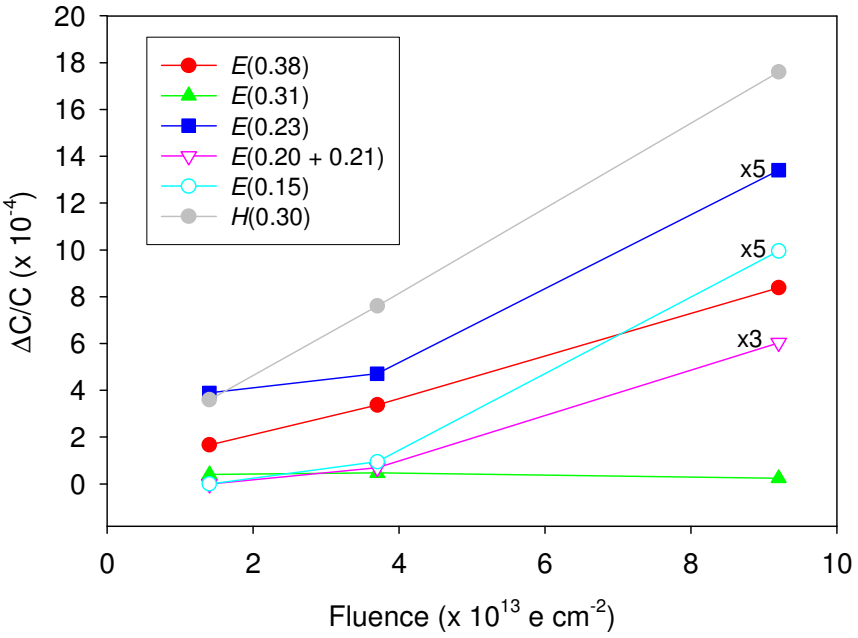

Fig. 8-2. Normalized DLTS peak height for each defect in the sample Ge100 as a function of fluence.

This proves that diode fabrication by resistive evaporation process does not introduce any detectable defect levels within semiconductor band gap. After irradiation with a fluence of 1.4 x 10^{13} e cm^{-2} a hole trap, *H*(0.30) is observed, curve (b_h) and *E*(0.38), *E*(0.31), *E*(0.23) trap levels are observable from curve (b_e). After a fluence of 9.2 x 10^{13} e cm^{-2}, three more electron traps *E*(0.21), *E*(0.20) and *E*(0.15) were introduced (curve (d_e)). Fig. 8-3 (a) depicts LDLTS spectra, for *E*(0.38), a single peak at 190 K and the peak shifted to higher emission rate at 200 K, which is consistent with a real defect level peak. In Fig. 8-3 (b), the LDLTS spectra for closely spaced levels *E*(0.21) and *E*(0.20) is shown as distinct peaks. At each temperature the extracted emission rates of the two peaks differs by a factor greater than 2 and both peaks shifted to higher emission rates when temperature was increased. The level *E*(0.38) and *H*(0.30) have been assigned to the vacancy – antimony (V-Sb) center, i.e. the so called *E*-center. This is further supported by the linear dependence of defect signal on fluence for both *E*(0.38) and *H*(0.30) as shown in Fig. 8-2. The *E*-center introduces three levels with different charge state in Ge band gap. *E*(0.38) is the double acceptor charge state (--/-) and *H*(0.30) is the single acceptor charge state (0/-) of the *E*-center [2-6]. The electron traps *E*(0.15), *E*(0.20), *E*(0.21), *E*(0.23) and

E(0.31) have not been identified, but only speculations that they are Sb and/or interstitial (I) related have been reported.

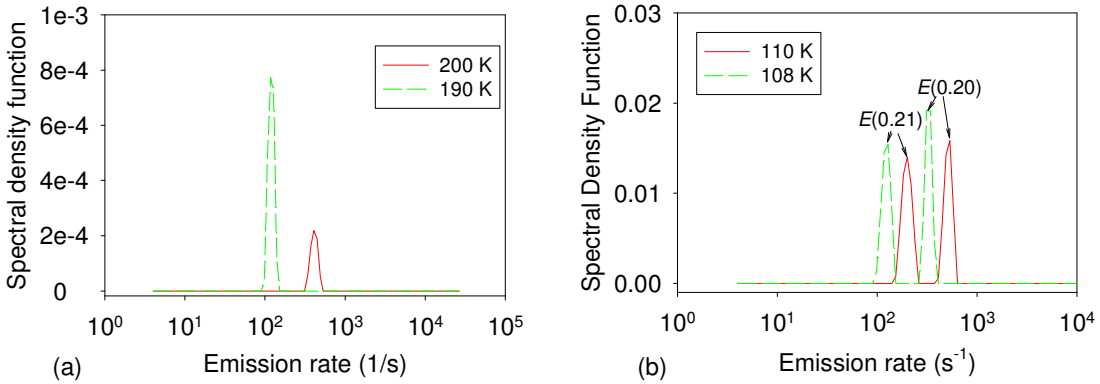

Fig. 8-3. LDLTS spectra for (a) E(0.38) as recorded at 190 K (dotted curve) and 200 K (solid curve) and (b) closely spaced traps E(0.20) and E(0.21) recorded at 108 K (dotted curve) and 110 K (solid curve). The spectra were recorded at a quiescent reverse bias of -1 V, filling pulse of 0 V and pulse width of 1 ms.

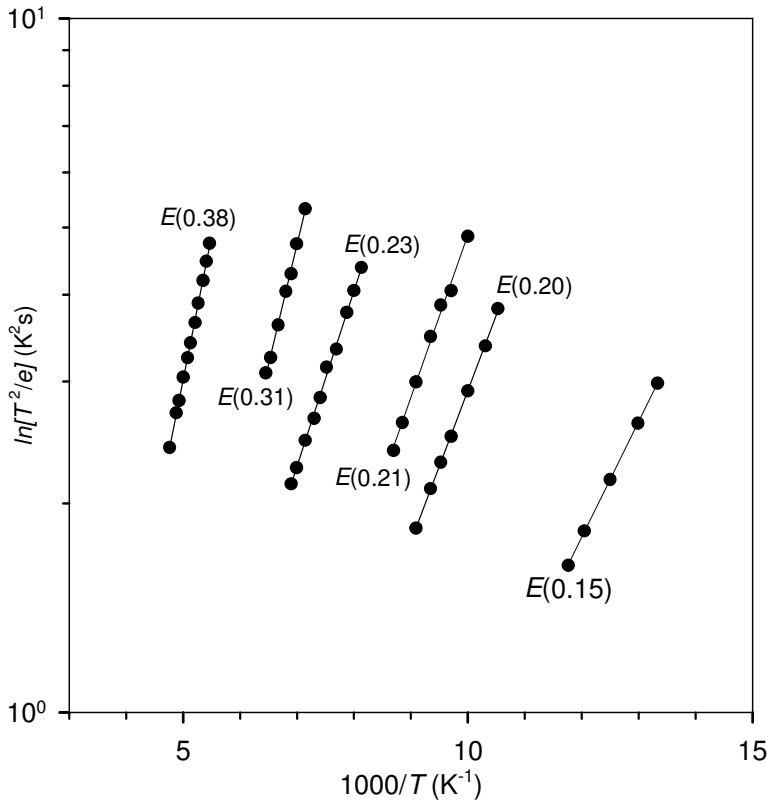

Fig. 8-4. Arrhenius plots of electron traps introduced in n-Ge after MeV electron irradiation.

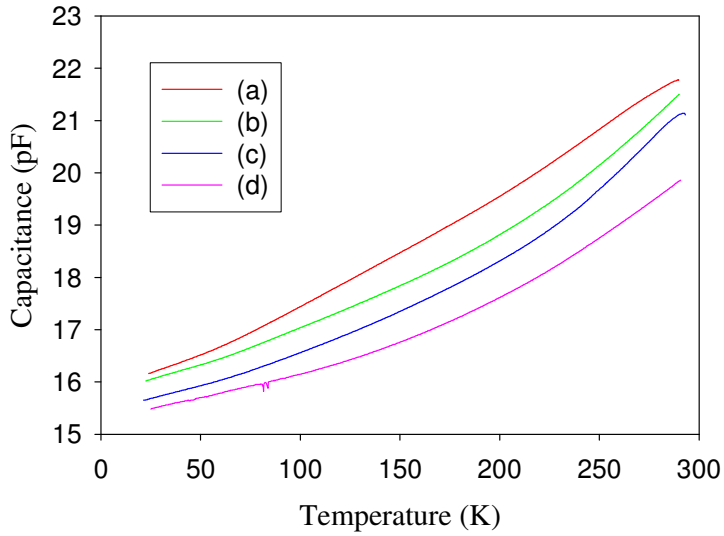

Fig. 8-5. Capacitance – temperature profiles of Ge110 for (a) as-deposited, and after irradiation with a fluence of (b) 1.4 x 10^{13} e cm^{-2}, (c) 9.2 x 10^{13} e cm^{-2} and (d) 1.7 x 10^{14} e cm^{-2} recorded at a quiescent reverse bias of -2 V.

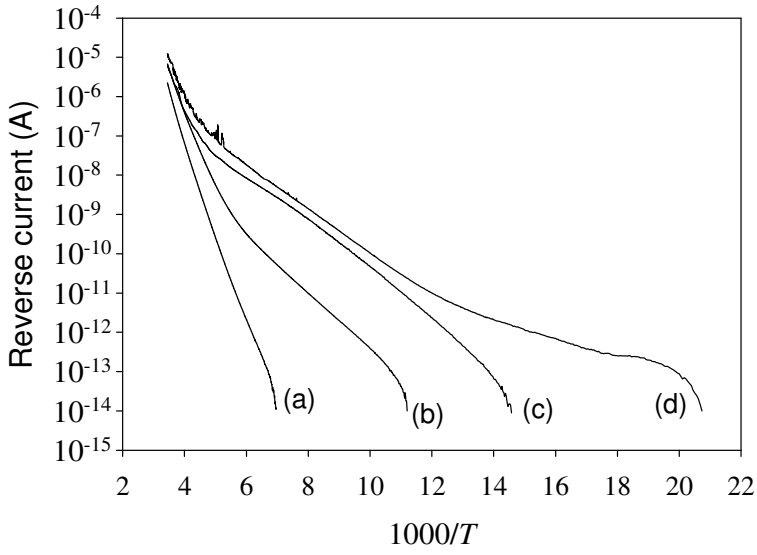

Fig. 8-6. Reverse current versus temperature profiles for Ge110 for (a) as-deposited, and after irradiation with a dose of (b) 1.4 x 10^{13} e cm^{-2}, (c) 9.2 x 10^{13} e cm^{-2} and (d) 1.7 x 10^{14} e cm^{-2} measured at a quiescent reverse bias of -1 V.

The normalized peak height signals for *E*(0.15), *E*(0.20), *E*(0.21), *E*(0.23) increase linearly with fluence within experimental error, suggesting that these traps are V or I related, while the defect concentration for *E*(0.31) is nearly independent of the dose, as shown in Fig. 8-2. Defect models are needed to identify this defect levels.

The diode capacitance – temperature (*C-T*) curves at various irradiation doses, depicted in Fig. 8-5, show a general shift to lower capacitance as the dose is increased, curves (a) – (d). This shows an increase in charge carrier traps with higher dose as expected. These results correlate well with the current-temperature (*I-T*) results shown in Fig. 8-6, which depict a near ideal behavior for the as-deposited sample, curve (a) and there is a shift to higher leakage currents as trap density increases with higher irradiation doses. Apart from the defect related leakage currents, (*I-T*) curves also show that the leakage current is thermally generated, i.e. from 10^{-6} A at room temperature to 10^{-12} A at 100 K as shown in Fig. 8-6 curve (b).

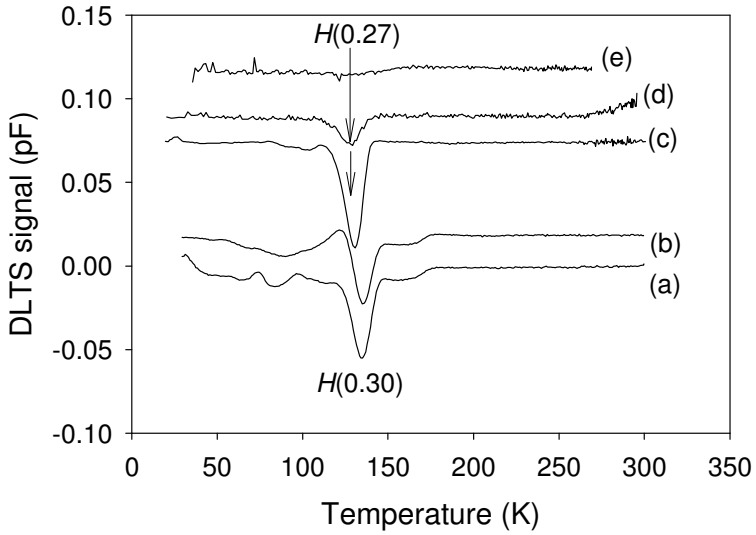

Fig. 8-7. DLTS hole traps spectra after irradiating Ge100 with electrons to a fluence of 1.7 x 10^{14} e cm^{-2} for (a) as-irradiated and after annealing at (b) 100˚C, (c) 200˚C, (d) 300˚C, and (e) 350˚C. These spectra were recorded at a rate window of 80 s^{-1} and quiescent reverse bias of -2 V with a filling pulse of 3 V and pulse width of 1 ms.

In order to extract more information on the defects in Ge, annealing studies were performed on the samples and the annealing temperatures (i.e. temperature at which a defect is removed) are summarized in Table. 8-1. *E*(0.15), *E*(0.20), *E*(0.21) and *E*(0.38), are all completely removed after annealing at 200˚C. *E*(0.31) and *E*(0.23) were removed after annealing at 125˚C and 175˚C respectively. The annealing profile of the hole traps is depicted in Fig. 8-7. A new hole trap *H*(0.27) is introduced at 200˚C as shown in the DLTS spectrum, in Fig. 8-7 curves (c) and is removed after annealing at 350˚C, as depicted by curve (e). It is interesting to note that apart from

observing the hole trap *H*(0.27) after annealing, it was also observed in the as-irradiated samples which had been stored at room temperature for more that a month. The origin of this secondary hole trap is still unclear at the moment, but Markevich *et al*, suggested that it might be a V-Sb_2 complex formed as a result of the annealing of the *E*-center [9].

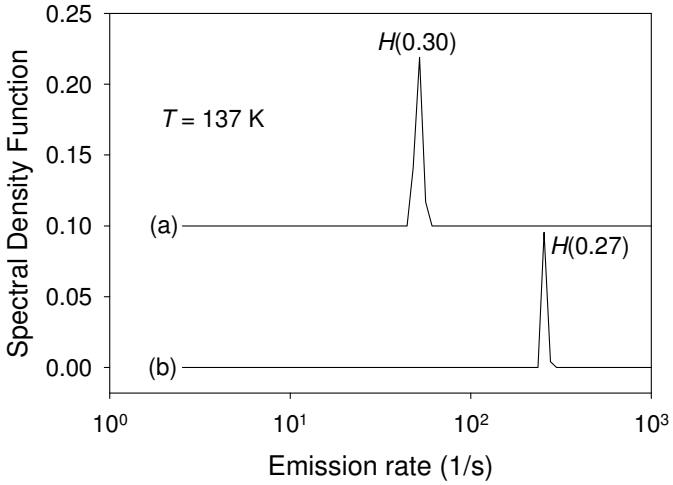

Fig. 8-8. LDLTS spectra for the hole traps H(0.27) and H(0.30) when recorded at 137 K (a) immediately after irradiation and (b) after annealing at 200˚C.

Fig. 8-8 shows the corresponding LDLTS signals for *H*(0.27) and *H*(0.30) both recorded at 137 K in as-irradiated sample (for *H*(0.30)) and in the sample annealed at 200˚C (for *H*(0.27)). The LDLTS spectra show two peaks with different emission rates, an indication that *H*(0.27) and *H*(0.30) are indeed different defect levels.

8.3.2 Dependence of electron irradiation induced defects in Ge on doping impurity density

DLTS spectra in Figs. 8-9 and 8-11 show the electron and hole traps introduced in three samples with different doping densities, respectively. As shown in Fig. 10, the defect concentration of *E*(0.38) linearly increases with doping density which confirms its assignment as V-Sb center. The concentrations of *E*(0.15), *E*(0.20) and *E*(0.21) increase with doping concentration (hence Sb-related), while *E*(0.23) and *E*(0.31) are independent of the doping concentration. A new low temperature peak *E*(0.04) is observed in the Ge110 sample. The origin of this particular defect is not clear at the moment. A summary of the electronic properties of the hole traps and a new electron

trap observed in the Ge110 samples are summarized in Table. 8.2 and the Arrhenius plots for the hole traps are depicted in Fig. 8-12.

Table 8.2. A summary of defects electronic properties introduced in n-type Ge by electron irradiation.

Defect	E_T (eV)	σ_a (cm^2)	T^a_{peak} (K)	T^b_{out} (˚C)	Defect origin
E(0.04)	$E_C - 0.04$	3.0 x 10^{-13}	30	200	I-related?
H(0.09)	$E_V + 0.09$	2.4 x 10^{-12}	47	225	$H_{0.09}$[b], V-Sb (+/0)[c]?
H(0.27)	$E_V + 0.27$	4.6 x 10^{-13}	135	325	V-Sb$_2$?
H(0.30)	$E_V + 0.30$	4.0 x 10^{-12}	142	225	V-Sb (0/-) [2-4]

[a]Peak temperature at a rate window of 80 s^{-1}, [b]see [ref. 2], [c]see [ref. 7].

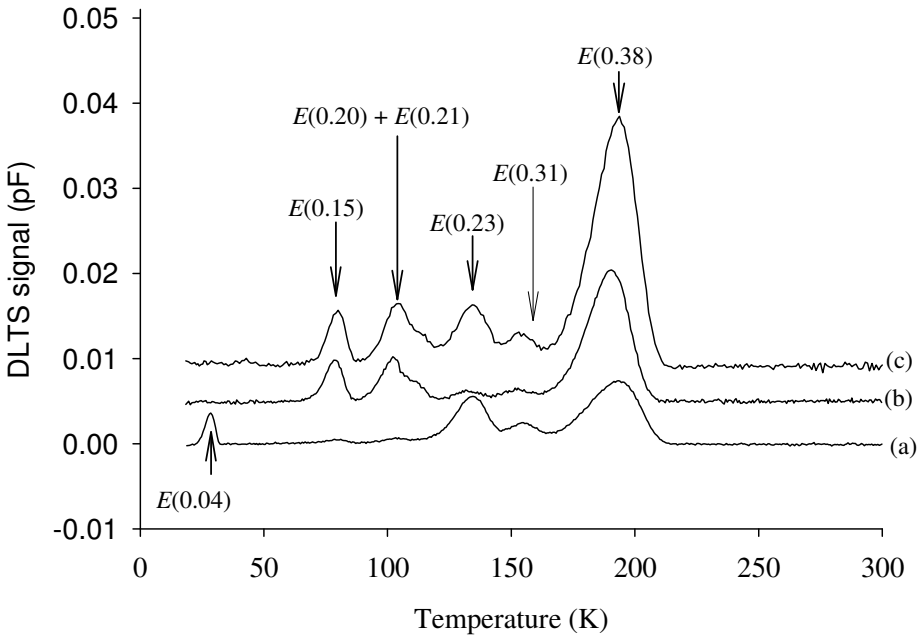

Fig. 8-9. Electron traps DLTS spectra for (a) Ge110 after a fluence of 3.7 x 10^{13} cm^{-2}, (b) Ge111 after a fluence of 9.2 x 10^{13} cm^{-2}, and (c) Ge100 after a fluence of 1.7 x 10^{14} cm^{-2}. The spectra were recorded at a quiescent reverse bias of -2 V, a filling pulse voltage of 0 V and +3 V for electron and hole traps respectively, and rate window of 80 s^{-1}.

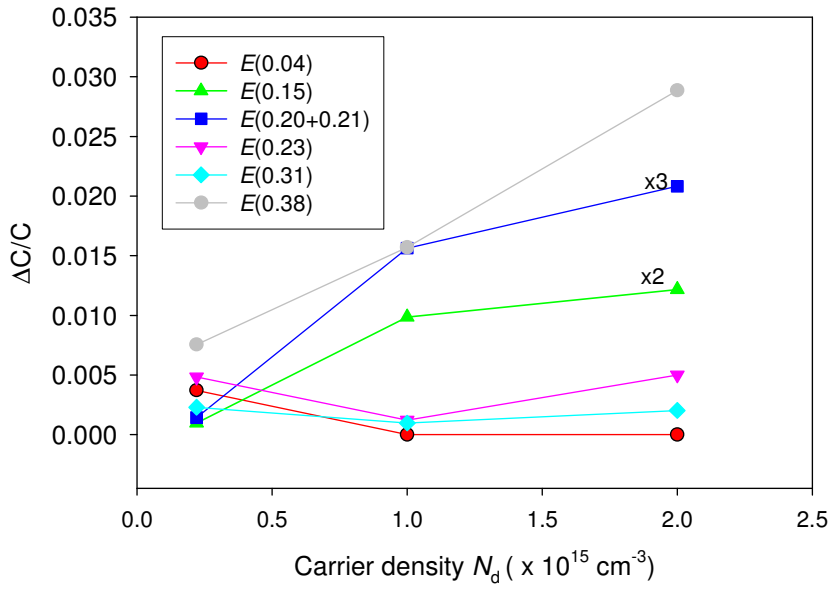

Fig. 8-10. Normalized DLTS peak height for each defect in the sample Ge100 as a function of fluence.

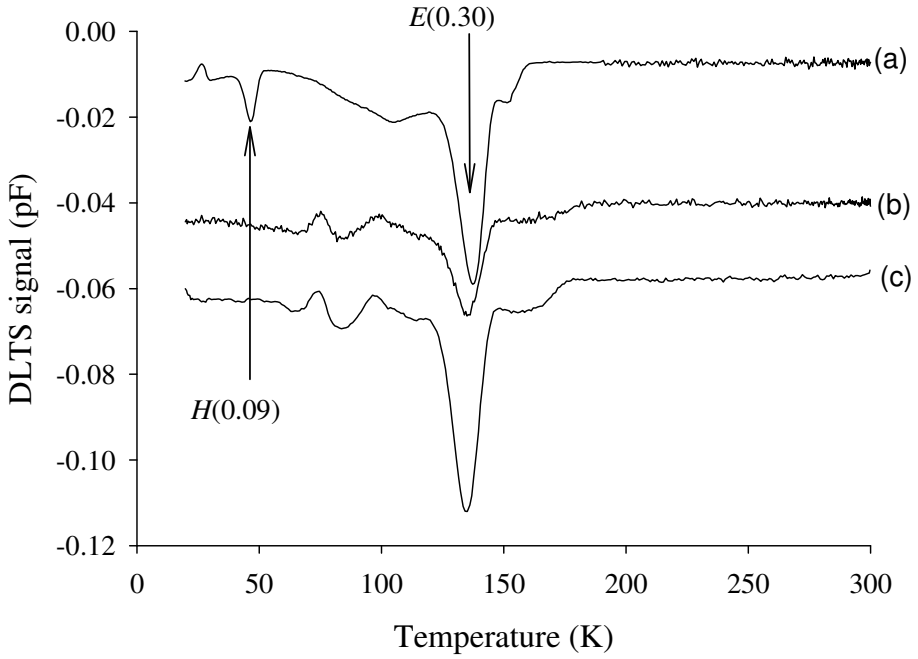

Fig. 8-11. Hole traps DLTS spectra for (a) Ge110 after a fluence of 3.7 x 10^{13} cm^{-2}, (b) Ge111 after a fluence of 9.2 x 10^{13} cm^{-2}, and (c) Ge100 after a fluence of 1.7 x 10^{14} cm^{-2}. The spectra were recorded at a quiescent reverse bias of -1 V, a filling pulse voltage of 0 V and +3 V for electron and hole traps respectively, and rate window of 80 s^{-1}.

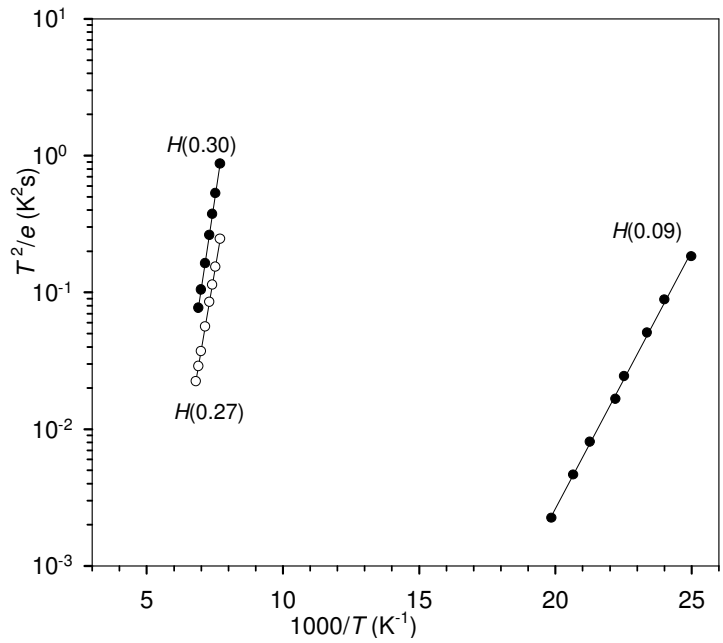

Fig. 8-12. Arrhenius plots of hole traps introduced in n-Ge after 1 MeV electron irradiation.

After annealing Ge110, the electron trap *E*(0.04) showed reverse annealing from room temperature upto 125˚C. Within the same temperature range there is a corresponding reduction in the concentration of the traps *E*(0.20), *E*(0.21), and *E*(0.31) which are probably interstitial related and this may suggest that *E*(0.04) is also interstitial related.

Defect concentration versus depth, i.e. depth profile of the *E*(0.38) measured in Ge100 is presented in Fig. 8-13. As clearly seen in the graphs, the defect concentration was generally constant with depth, which proves that the defect introduction was as result of energetic light particles such as electrons. The profiles shifted to higher concentrations as the fluence was increased as more damage was introduced into the material. The defect concentration of *E*(0.38) increased linearly with fluence upto the maximum fluence used in this study, as illustrated in Fig. 8-13 and 8-14, which can be explained by the fact that as more damage is induced into the material then there are more vacancies to combine with antimony to form the V-Sb center. The calculated introduction rate for this defect level is 1.6 x 10^{1} cm^{-1}.

8.3.3 Thermal stability of defects in Ge at room temperature

The thermal stability of primary defects at room temperature has been investigated. Fage-Pedersen *et al* [4] have showed that several defects in Ge evolve at room temperature. Curves of reverse current (at -1 V) versus fluence measured after different storage times are shown in Fig. 8-15.

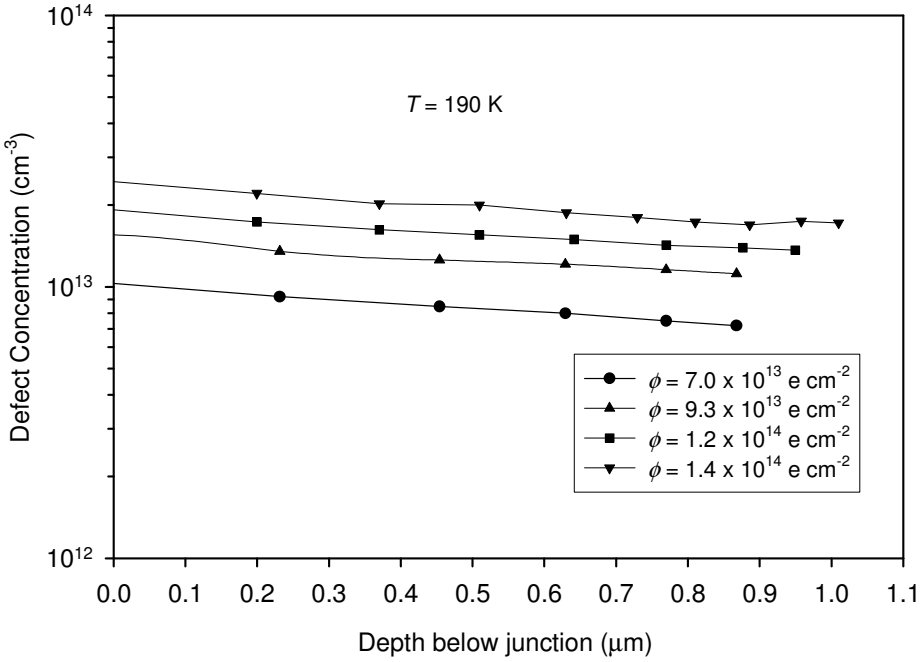

Fig. 8-13. Defect depth profile for E(0.38) as measured in Ge100 sample at fluence 7.0 x 10^{13} e cm^{-2}, 9.3 x 10^{13} e cm^{-2}, 1.2 x 10^{14} e cm^{-2}, and 1.4 x 10^{14} e cm^{-2}. The data was measured at a quiescent reverse bias of -5 V, a varying pulse voltage and pulse width of 1 ms (ref. 10).

There is a sudden decrease of reverse current after the electron irradiation. This can be attributed to an increase in the effective barrier height associated with the reduction of free carriers as a result of capturing by the introduced displacement damage. After increasing the fluence, there is a general increase in reverse current due to increase in traps which may act as generation-recombination centers, thereby increasing the leakage current. After each irradiation, the reverse current – fluence curves shifted to higher leakage current for longer storage time. This is due to increased defect concentration which evolves over time at room temperature as depicted in the DLTS spectra in Fig. 8-16.

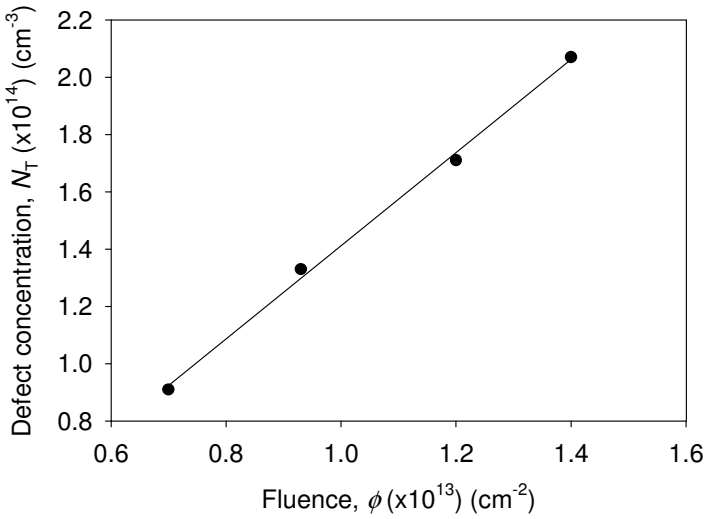

Fig. 8-14. Defect concentration of E(0.38) as a function of dose from which defect introduction rate is deduced.

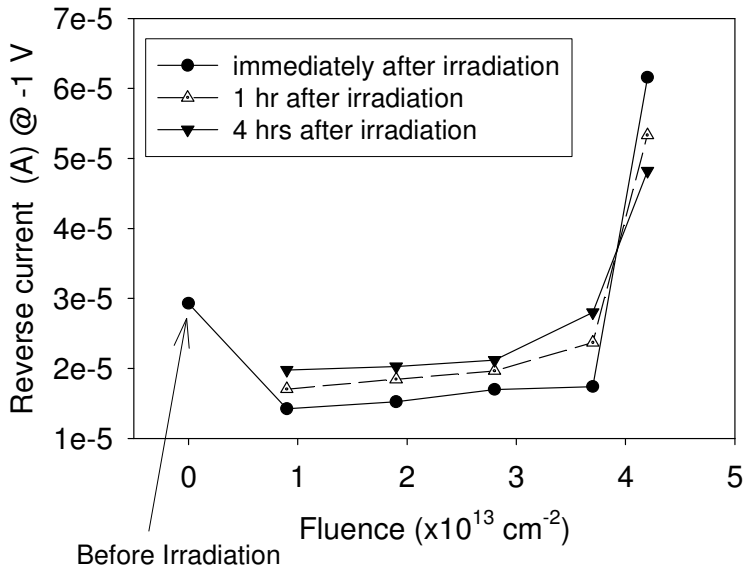

Fig. 8-15. The diode reverse current at -1 V reverse bias versus fluence, recorded immediately after irradiation, 1 hr, and 4 hrs after irradiation for Ge100.

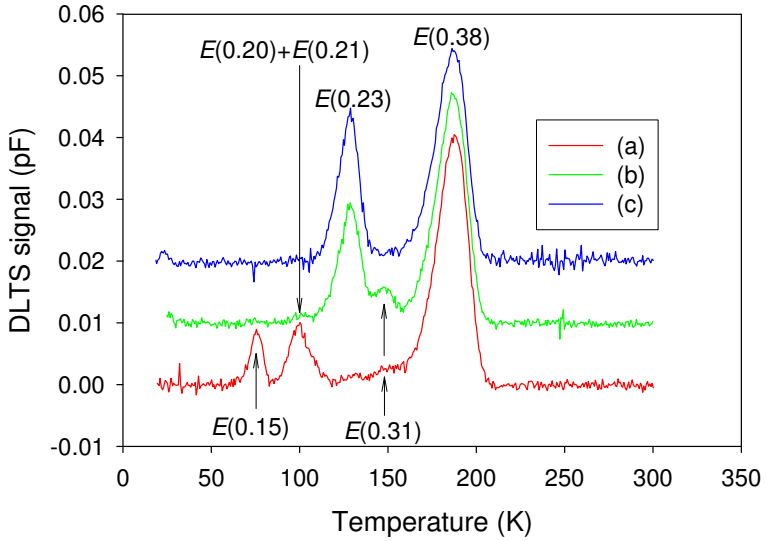

Fig. 8-16. DLTS spectra for Ge110 after electron irradiation with a fluence of 1.4 x 10^{14} e cm^{-2} when recorded, (a) immediately, (b) 2 days, and (c) 2 weeks after irradiation. The spectra were recorded at a quiescent reverse bias of -2 V, a filling pulse voltage of 0 V, and a rate window of 80 s^{-1}.

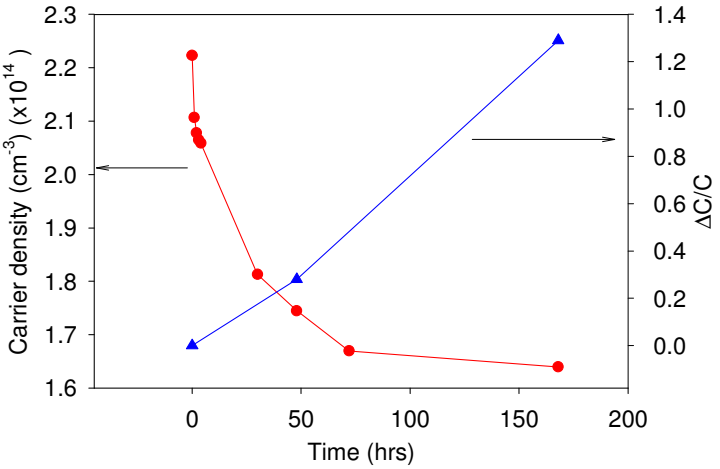

Fig. 8-17. Carrier concentration after irradiation of Ge110 with a fluence of 3.7 x 10^{13} e cm^{-2} as monitored over a period of time.

The concentration of *E*(0.31), *E*(0.23) increases significantly in the first 2 days after the irradiation, whereas there is a decrease in concentration of *E*(0.15), *E*(0.20), *E*(0.21) and *E*(0.38) in the same period. Similarly to the DLTS spectra recorded over a period of time, the free concentration shows a rapid decrease in the first day after irradiation and then the decrease slows down after 3 days and this correlates well with increase of the of *E*(0.23) which was monitored over time the same time period.

8.4 Summary and conclusions

Defects introduced in Ge doped with antimony have been characterized by DLTS and LDLTS. Electron traps *E*(0.15), *E*(0.20), *E*(0.21), *E*(0.23), *E*(0.31) and *E*(0.38), and hole traps *H*(0.09), *H*(0.27) and *H*(0.30) have been observed in electron irradiated Ge samples. Traps *E*(0.38), *H*(0.30) and *H*(0.09) have been identified as the three charge states of the V-Sb (*E*-center), namely, double acceptor (--/-), single acceptor (-/0), and single donor (0/+), respectively. Although the *ab initio* density functional theory (DFT) calculations has shown that divacancy has a single donor level at 0.08 eV and an acceptor level 0.3 eV above the valence band [11] and that the divacancy anneals at values between 150-180˚C [12], there has not been any experimental evidence of this from DLTS measurements. There are generally two ways of divacancy formation in semiconductors, i.e. (i) as a primary defect when the energy of irradiating particle is high enough or (ii) by the association of two single vacancies. The vacancy in Ge is negatively charged in a broad interval of Fermi level position in the gap [13], therefore the later mechanism of divacancy formation in Ge is suppressed because of coulombic repulsion of vacancies. Assuming direct divacancy formation then it means the complex is very unstable at room temperature and it will quickly dissociate. Kolkovsky *et al* [14] proposed that absence of a divacancy is due to the divacancy recombining with the self- interstitials rather than by dissociation.

It has been shown that after electron irradiation, some of the defects created evolve and only become fairly stable after at least 7 days of room storage. The *E*(0.23) peak height was observed to increase significantly a day after irradiation. Upon annealing, it has been observed that all defects in Ge are removed after a low thermal budget (350 - 400˚C) when compared to defects in Si. A new hole trap has been observed after annealing at 200˚C or after room temperature storage for a month. The identity of this new hole trap is currently subject to speculation.

The depth profile of the *E*(0.38) showed a uniform defect concentration with depth. This proves that high energy electrons introduces well spaced vacancies and interstitial and hence form stable complexes which are uniform with depth. The calculated introduction rate for the trap *E*(0.38) is 1.6×10^{1} cm^{-1} which is consistent with electron irradiation induced defects.

References

[1] Germanium Silicon, Phyiscs and Materials, Semiconductor and Semi-metals Vol. 56, edited by Hull and J. C. Bean (Academic, San Diego, 1999).

[2] F.D. Auret, W.E. Meyer, S. Coelho and M. Hayes, *Appl. Phys. Lett*. **88**, 242110 (2006).

[3] F.D. Auret, P.J. Janse van Rensburg, M. Hayes, J.M. Nel, W.E. Meyer, S. Decoster, V. Matias and A. Vantomme, *Appl. Phys. Lett*. **89**, 152123 (2006).

[4] J. Fage-Pedersen, A. Nylandsted Larsen and A. Mesli, *Phys. Rev. B*. **62**, 10116 (2000).

[5] V.P. Makervich, I.D. Hawkins, A.R. Peaker, K.V. Emstev, V.V. Emstev, V.V. Litvinov and L. Dobaczewski, *Phys. Rev. B*. **70**, 235213 (2004).

[6] V.P. Makervich, A.R. Peaker, V.V. Litvinov, V.V. Emstev and L.I. Murin, *J. Appl. Phys.* **95**, 4078 (2004).

[7] C.E. Lindberg, J. Lundsgaard Hansen, P. Bomholt, A. Mesli, K. Bonde Nielsen and A. Nylandsted Larsen, *Appl. Phys. Lett*. **87**, 172103 (2005).

[8] A.R. Peaker, V.P. Markevich, L.I. Murin, N.V. Abrosimov and V.V. Litvinov, *Mater. Sci. Eng*. **B 124** (2005) 166.

[9] V. P. Markevich, *Mater. Sci. in Semicond. Process*. **9** (2006) 589.

[10] Y. Zohta and M.O. Watanabe, *J. Appl. Phys*. **53** No.**3** (1982) 1809.

[11] J. Coutinho, R. Jones, V.J.B. Torres, M. Barroso, S. Oberg and P.R. Briddon, *Appl. Phys. Lett*. **88** (2006) 095208.

[12] H.J. Stein, '*Divacancy-like absorption in ion-bombarded Ge',* In: Radiation damage and defects in Semiconductors. London, London Institute of Physics: 1973.

[13] H. Haesslein, R. Sielemann and C. Zistl, *Phys. Rev. Lett*. **80** (1998) 2626.

[14] V.L. Kolkovsky, M. Christian Petersen, A. Nylandsted Larsen and A. Mesli, *Mater. Sci. in Semicond. Process*., (2008), doi: 10.1016/j.mssp.2008.07.006.

List of Publications

1. Cloud Nyamhere, M. Das, F.D. Auret and A. Chawanda, "*A Study of electron induced defects in n-type germanium by Deep Level Transient Spectroscopy (DLTS)",* Phys. Stat. Sol. (c) vol. 5, No. 2**,** (2008), 623 – 625.
2. C. Nyamhere, F.D. Auret, A.G.M. Das and A. Chawanda, "*A study of the dependence of electron-induced defects on the doping impurity density in n-type germanium by deep-level transient spectroscopy (DLTS)*", Physica B; Vols 401- 402 (2007) 499-502.